ICSV18
RIO DE JANEIRO
BRAZIL
18TH INTERNATIONAL CONGRESS ON SOUND & VIBRATION 10–14 JULY 2011

AN ANALYSIS OF MESH PARAMETERS OF A VISCOTHERMAL ACOUSTIC FE MODEL

Gustavo C. Martins, Júlio A. Cordioli, Roberto Jordan

Department of Mechanical Engineering, Federal University of Santa Catarina, 88090-400, SC, Brazil, e-mail: martins_gustavo@ymail.com

Analytical solutions for viscothermal acoustic problems are available only for very simple systems. The solution of more complex geometries and boundary conditions requires the use of numerical techniques, and this type of approach is still absent in vibro-acoustic commercial codes. Recently, numerical viscothermal acoustic models have been proposed in the literature that allow the analysis of arbitrary geometries. These models are obtained by using the Finite Element (FE) method, but the computational cost of its solution can be considerably high. This problem has led to an analysis of the mesh parameters of a viscothermal acoustic model in order to minimize the computational costs of the solution for a given level of precision.

1. Introduction

The acoustic analysis of miniaturized devices such as hearing aids presents additional complexities which limit the use of standard acoustic models. These difficulties are due to the small dimensions of acoustic waveguides within these systems, where the phenomena of viscous friction and thermal diffusion affect the acoustic propagation. These phenomena are called in literature by acoustic viscothermal effects and are neglected in standard acoustic models. The inclusion of viscothermal effects in acoustic models adds complexity, and the analytical solution of the problem is only possible for simple cases.

Viscothermal acoustic models can be obtained from the conservative equations where the terms of viscosity and thermal conductivity of the fluid are present. The analytical solution of this system of equations is possible only in specific cases.[1,2] The Low Reduced Frequency (LRF) model, obtained for the first time by Zwikker and Kosten,[3] provides direct analytical solutions for simple geometries through simplifications and assumptions about the geometry, boundary layer thickness and wavelength.[2] For tubes, the LRF model has been compared against other analytical models by Tijdeman,[4] who showed that this model overcome some of the limitations of previous models for this type of geometry. In fact, for simple geometries and boundary conditions, the LRF model can be considered accurate when the acoustic wavelength is large compared with the problem length scale the boundary layer thickness. However, to solve complex geometries or boundary conditions, a numerical solution method is needed. The LRF model was already implemented numerically through the Finite Element (FE) method.[2] The FE formulation of the LRF model only enables the solution of coupled problems, but it is not apropriate to solve complex geometries due to the LRF model assumptions.

The implementation of a more general viscothermal acoustic model using FE has been previously published by Malinen,[5] Nijhof[6] and Kampinga.[7] No geometric restrictions are imposed on these models. However, this advantage does lead to an increase in computational effort to solve the

model. These FE formulations have not only the pressure, but also the temperature and the velocity vector as degrees of freedom. Furthermore, it needs much finer mesh on the boundary layer to get accurate results.

The aim of this paper is to assess how to properly define the mesh of the problem in order to reduce the computational effort associated with the solution of a FE viscothermal acoustic model. The paper starts with a review of the viscothermal acoustic model and its weak formulation in Section 2, which is used in the FE implementation Next, the analysis of the mesh parameters is presented, and the results are discussed in Section 3. The FE formulation was implemented using the commercial FE software COMSOL.[8]

2. Viscothermal acoustic model

The basic equations governing the propagation of sound waves are the equation of continuity, the momentum equation, the energy equation and the equation of state (an ideal gas will be assumed). In the absence of mean flow, gravitational forces and energy sources, these equations can be all linearized by assuming small harmonic perturbations and can be written as

$$i\omega\rho_0\boldsymbol{u} + \boldsymbol{\nabla}p = (\lambda + 2\mu)\boldsymbol{\nabla}(\boldsymbol{\nabla}\cdot\boldsymbol{u}) - \mu\boldsymbol{\nabla}\times(\boldsymbol{\nabla}\times\boldsymbol{u}), \tag{1a}$$

$$i\omega\rho_0 C_v\tau + P_0\boldsymbol{\nabla}\cdot\boldsymbol{u} = \kappa\Delta\tau, \tag{1b}$$

$$i\omega\rho + \rho_0\boldsymbol{\nabla}\cdot\boldsymbol{u} = 0, \tag{1c}$$

$$p = R_0(\rho_0\tau + \rho T_0), \tag{1d}$$

where ω é angular frequency, p is acoustic pressure, $\boldsymbol{u}$ is the particle velocity vector, τ is acoustic temperature, ρ is acoustic density, P_0 is mean pressure, T_0 is mean temperature, ρ_0 is mean density, λ is the dilatational viscosity coefficient, μ is the shear viscosity coefficient, C_v is the specific heat at constant volume, κ is the heat conduction coefficient and R_0 is the gas constant.

As mentioned before, the analytical solution of this system of equations is only possible for simple geometries, and it is necessary to rely on numerical method to solve more complex problems. The FE method is the main numerical method used for this task. Before the FE implementation, the Eqs. (1) are usually written as a mixed formulation.[7] The linearized momentum equation (1a) is then rewritten as:

$$i\omega\rho_0\boldsymbol{u} + \boldsymbol{\nabla}p = \boldsymbol{\nabla}\cdot\Phi, \tag{2}$$

where Φ denote the viscous stress tensor,[7] given by

$$\Phi = \lambda(\boldsymbol{\nabla}\cdot\boldsymbol{u})I + \mu\left(\boldsymbol{\nabla}\boldsymbol{u} + (\boldsymbol{\nabla}\boldsymbol{u})^T\right), \tag{3}$$

where I is the identity tensor.

Substituting Eq. (1d) in Eqs. (1b) and (1c), the mixed formulation is given by

$$i\omega\rho_0\boldsymbol{u} + \boldsymbol{\nabla}p = \boldsymbol{\nabla}\cdot\Phi, \tag{4a}$$

$$i\omega\rho_0 C_p\tau - i\omega p = \kappa\Delta\tau, \tag{4b}$$

$$i\omega\left(\frac{p}{P_0} - \frac{\tau}{T_0}\right) + \boldsymbol{\nabla}\cdot\boldsymbol{u} = 0, \tag{4c}$$

where C_p denotes specific heat at constant pressure.

For each boundary of the problem, it is necessary to specify thermal and mechanical boundary conditions which, together with Eqs. (4), lead to the formulation in the "strong" form. In the present implementation, the FE method is used to approximate the solution based on the formulation in the

"weak" form. In this case, the formulation is obtained by using a Galerkin approach where Eqs. (4) are multiplied by the weighing functions $\boldsymbol{u}^w$, τ^w and p^w respectively, and integrated over the domain Ω. By using partial integration and the Gauss theorem the weak form is given by[7,9]

$$\int_\Omega i\omega\rho_0 \boldsymbol{u}^w \cdot \boldsymbol{u} - (\boldsymbol{\nabla}\cdot\boldsymbol{u}^w)p + \boldsymbol{\nabla}\boldsymbol{u}^w : \Phi \; d\Omega + \int_{\partial\Omega} \boldsymbol{u}^w \cdot \boldsymbol{h}_M \; d\partial\Omega = 0, \tag{5a}$$

$$\int_\Omega i\omega\rho_0 C_p \tau^w \tau - i\omega\tau^w p + \kappa\boldsymbol{\nabla}\tau^w \cdot \boldsymbol{\nabla}\tau d\Omega - \int_{\partial\Omega} \tau^w h_T \; d\partial\Omega = 0, \tag{5b}$$

$$\int_\Omega \frac{i\omega}{P_0} p^w p - \frac{i\omega}{T_0} p^w \tau + p^w \boldsymbol{\nabla}\cdot\boldsymbol{u} \; d\Omega = 0. \tag{5c}$$

In the Galerkin approach, the weighing functions are the same shape functions used for the corresponding degrees of freedom. In the present study, quadratic functions were used as shape functions for τ, τ^w, $\boldsymbol{u}$ and $\boldsymbol{u}^w$ and linear shape functions for p and p^w. It has been shown in the literature that this combination of shape functions results in a stable element.[9]

3. Analysis of the mesh parameters

3.1 Initial analysis

The solution of the system of equations described in Section 2 by means of the FE method (called here the Linearized Navier-Stokes-Fourier approach, LNSF) involves four variables in a 2D problem (u_x, u_y, p and τ) and five variables in a 3D problem (u_x, u_y, u_z, p and τ). The number of degrees of freedom is also increased by the use of quadratic shape functions. As a consequence, the computational cost of a viscothermal acoustic model can be considerably higher than a standard acoustic model.

Another aspect of the discretization of a LNSF model can be observed by plotting the analytical solution[4] for u_x along the radius of a simple tube when a viscothermal acoustic wave propagate through the tube (Fig. 1). It is possible to observe that there are large variations of the particle velocity near the walls due to the fluid viscosity. Therefore, the FE discretization of the system must be sufficiently refined to get an accurate description of the velocity field, which increases even further the computational costs of the numerical solution of the LNSF . Consequently, the definition of the mesh of a LNSF model is a very important step of the modeling process and requires special attention in order to ensure the convergence of the results with a minimum solution time.

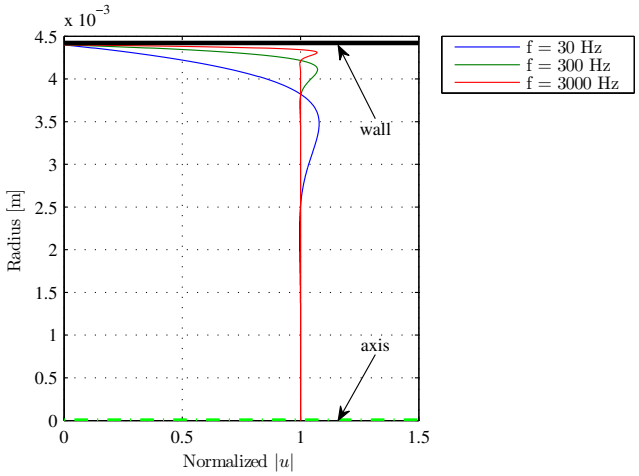

Figure 1. Normalized magnitude of particle velocity along radius of a tube with diameter of 8.8 mm.

A first example is used to emphasize the importance of the definition of an appropriate mesh for a LNSF model. The viscothermal acoustic propagation through a tube with 200 mm length and 8.8 mm diameter is considered. A 2D-axisymmetric representation of the problem is used in order to reduce computational costs. The model can provide an initial idea of the relation between mesh, convergence of results and computational costs. As shown in Fig. 2 (only a portion of the tube is shown), four different meshes were used for the problem: (i) 0.88 mm squared element, (ii) 0.44 mm square element, (iii) 0.22 square element, and (iv) a rectangular element with a a refined discretization closer to the wall.

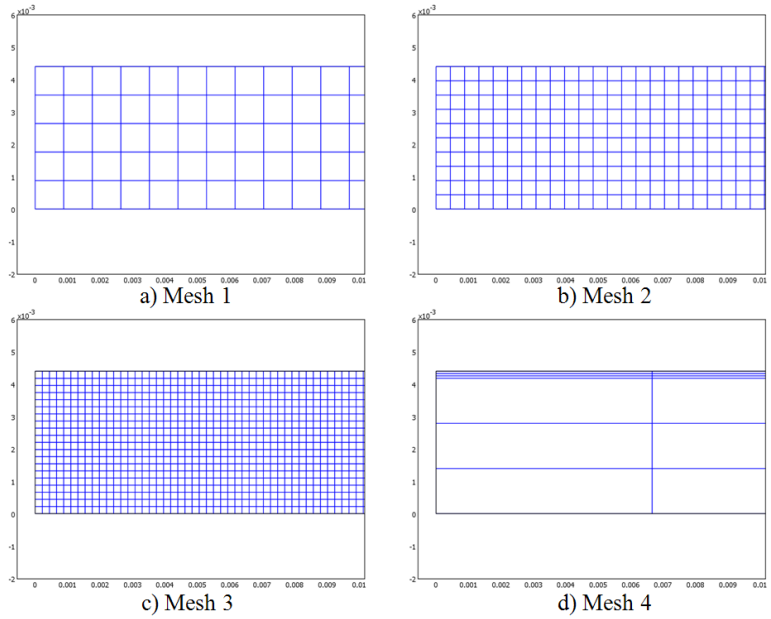

Figure 2. Meshes used for the initial tests of LNSF model solution.

The tube wall was assumed isothermal, while a prescribed adiabatic acoustic pressure was applied to one end of the tube and an adiabatic unbaffled piston radiation impedance was applied to the other end. The transfer function $H(f)$ between the prescribed acoustic pressure and the acoustic pressure on the other end of the tube was used to evaluate the convergence of the model. Fig. 3.a compares the curves for the magnitude of $H(f)$ obtained with each mesh, together with analytical solution given by the so-called Low Reduced Frequency model (LRF)[2,4] . Processing times are also provided in Fig. 3. Taking the LRF model as reference, a error function was defined as

$$\epsilon_p(f) = \frac{||H(f)| - |H_{ref}(f)||}{|H_{ref}(f)|}, \tag{6}$$

where $|H(f)|$ and $|H_{ref}(f)|$ are the transfer function between pressures at each end of the tube obtained by LNSF and LRF models, respectively.

In Fig. 3, it can be seen that in general the error obtained with the finest square mesh (Mesh 3) shows higher values than the error obtained with Mesh 4, while the processing time of the Mesh 4 was more than a 100 times smaller than the one observed for Mesh 3. Clearly, the use of some knowledge about the fields being solved by the LNSF model to define the mesh can considerable reduce the solution time of the analysis and improve the convergence of the results.

3.2 Parametrization of the mesh

In order to analyze the discretization of a LNSF model, the problem analyzed in the previous section (pressure transfer function of a simple tube) was again considered since it has an analytical

solution. In view of the behaviour observed for the particle velocity field in Fig. 1, the problem domain was divided into two regions: (i) the acoustic boundary layer and (ii) the mainstream region, so that each subdomain could be meshed differently. The linear behaviour of the particle velocity and temperature in the mainstream region allows a reduced number of elements to be used in this region, while the strong gradient observed for the field variables in the acoustic boundary layer requires a refined mesh. After the domain division, the creation of the meshes was controlled by the parameters shown in Fig. 4, where: L is the tube length, t is the thickness of elements in the acoustic boundary layer, h is the thickness of elements in the mainstream, R is the mainstream thickness, l is the length of all elements and δ'_t is the acoustic boundary layer thickness.

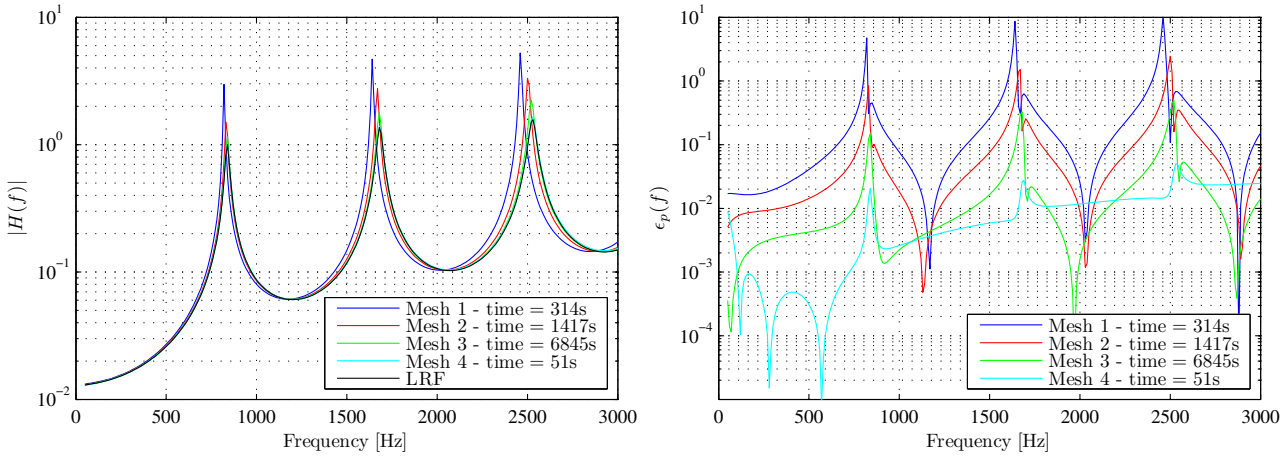

Figure 3. Magnitude of transfer functions (a) and error functions (b) calculated with the FE meshes of Fig. 2.

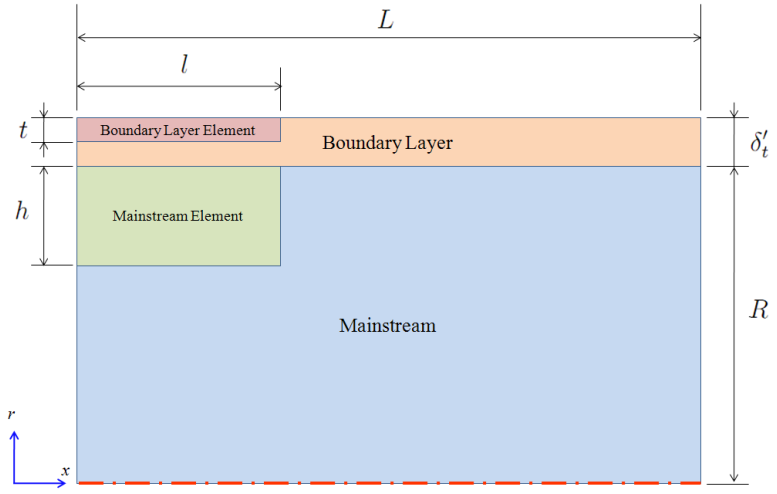

Figure 4. Mesh parameters for discretization study.

The thickness of the acoustic boundary layer is derived by Blackstock,[10] and is given by

$$\delta_v = \sqrt{\frac{2\mu}{\omega\rho_0}}, \tag{7}$$

$$\delta_t = \frac{\delta_v}{\sqrt{Pr}}, \tag{8}$$

where δ_v is the viscous acoustic boundary layer thickness, δ_t is the thermal acoustic boundary layer thickness and Pr is the Prandtl number. However, the boundary layer thicknesses given by Eqs. (7)

and (8) do not cover the whole region where large variations of acoustic temperature and particle velocity occur. This is due to the definition of the boundary layer thickness adopted by Blackstock,[10] which is the distance from the wall necessary for the particle velocity to achieve $1/e$ of its mainstream value. To better identify the desired region, an alternative definition of the boundary layer thickness was adopted so that it covers the distance from the wall to the point where the particle velocity achieves 99% of the mainstream value, or

$$\delta'_v = -\ln(1/100)\sqrt{\frac{2\mu}{\omega\rho_0}} = -\ln(1/100)\delta_v, \tag{9}$$

$$\delta'_t = \frac{\delta'_v}{\sqrt{Pr}}. \tag{10}$$

The acoustic temperature behaves similarly to the particle velocity, but with a slightly thicker boundary layer. Therefore, in this study the acoustic thermal boundary layer thickness given by Eq. (10) will be used to define the boundary layer subdomain shown in Fig. 4.

As can be noted by Eq. (9), the acoustic boundary layer thicknesses is inversely proportional to frequency, so that the boundary layer is very small at higher frequencies. Therefore, the frequency of the analysis also becomes a parameter of the discretization of the boundary layer region.

3.3 Analysis of the boundary layer discretization

As previously mentioned, the thickness of the boundary layer is inversely proportional to the frequency of analysis. Therefore, the maximum frequency of the analysis is the most critical case for the boundary layer discretization since it needs smaller elements in the boundary layer than lower frequencies. However, adopting the boundary layer thickness of the highest frequencies leads to a mesh that may not properly describe the particle velocity field at lower frequencies as the elements are confined to only an small region of the actual boundary layer.

In order to investigate this effect, two discretization scenarios were tested: (i) using the boundary layer of the maximum frequency for the whole frequency range, and (ii) redefining the mesh at each frequency step using the actual boundary layer thickness calculated using Eq. (10). In each case, the discretization of the boundary layer thickness was gradually increased while the discretization in the mainstream and in the length direction of the tube were kept constant with mesh parameters equal to: $l = L/100$ and $h = R$ (see Fig. 4). Examples of the meshes generated for case 2 can be seen in Fig. 5, while Fig. 5(c) was the mesh used for the whole frequency range in case 1.

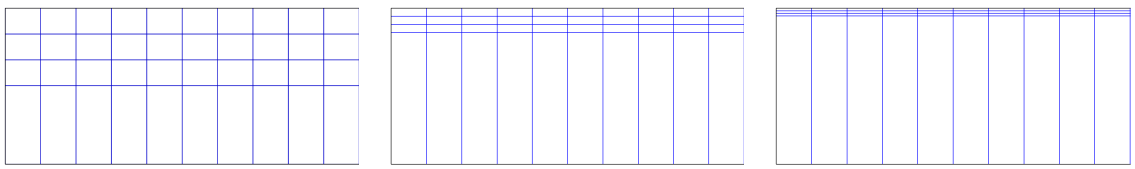

(a) f = 30 Hz (b) f = 300 Hz (c) f = 3000 Hz

Figure 5. Parameterized meshes with 3 elements along δ'_t.

The error as a function of frequency for the case with the fixed boundary layer thickness is shown in Fig. 6(a). As expected, it can be seen that increasing the number of elements in the boundary layer only reduces the error at higher frequencies. At low frequencies, only a small reduction of error is obtained, since the new elements are confined to restricted region of the actual boundary layer. The

results for a parameterized boundary layer thickness discretization can be seen in Fig. 6(b), where a uniform reduction of the error over the whole frequency range can be observed. This results justify the recommendation for the use of parametrized meshes based on frequency and the boundary layer thickness.

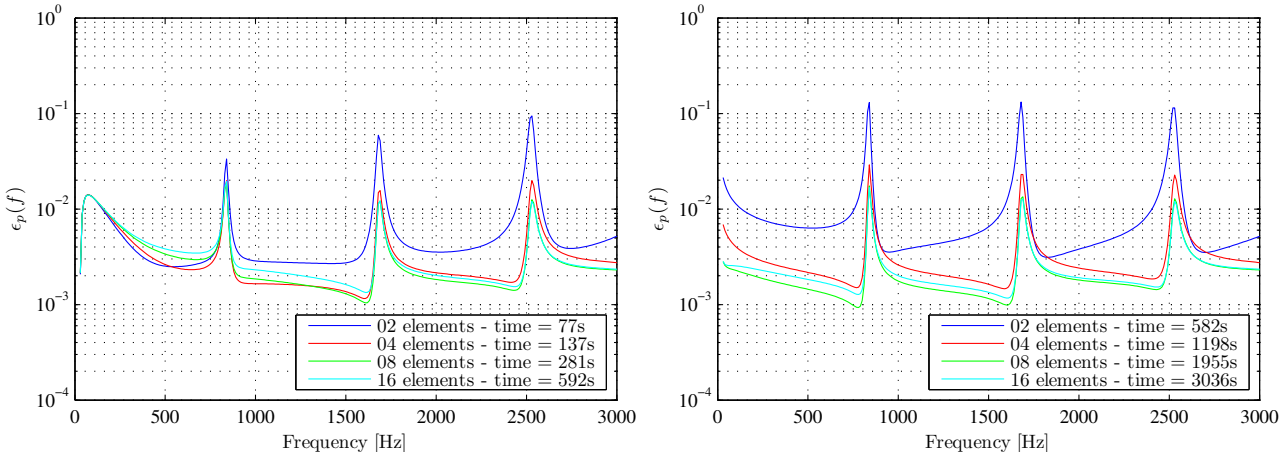

(a) Fixed mesh (b) Parameterized mesh

Figure 6. The ϵ_p functions for different number of elements along δ'_t.

3.4 Analysis of tube length and mainstream discretization

In this section, the effects of the discretization along the tube length and mainstream region are considered. The error ϵ_p was evaluated for different numbers of elements along the length of the tube, while other mesh parameters were kept fixed ($t = \delta'_t/8$ and $h = R$, assuming the boundary layer thickness of the maximum frequency). Likewise, the analysis of the mainstream thickness discretization was performed varying the number of elements along R and keeping fixed the other parameters ($t = \delta'_t/8$ and $l = L/100$). Fig. 7(a) shows the results for the error with increasing number of elements over the tube length.

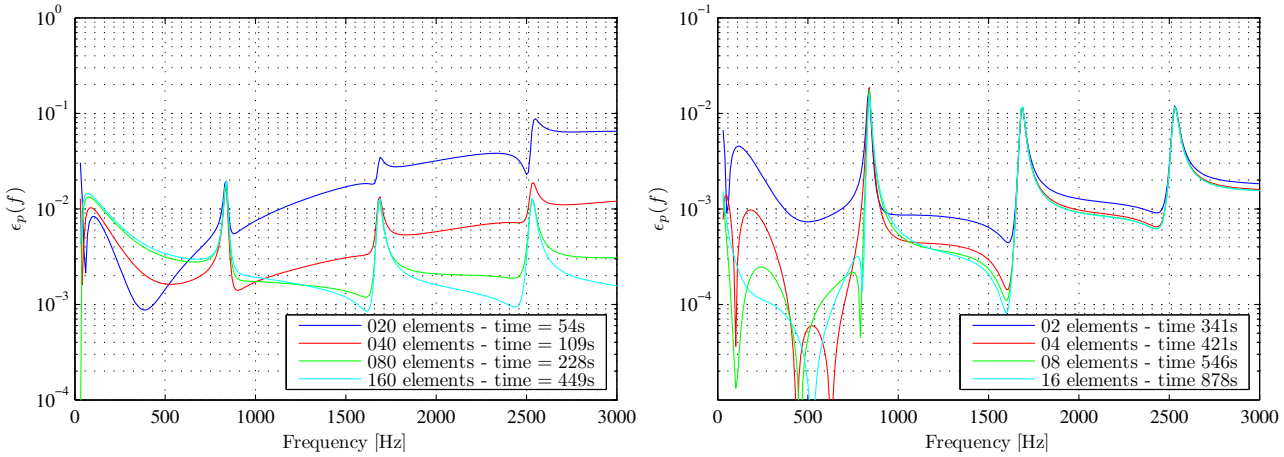

(a) (b)

Figure 7. The ϵ_p functions for different number of elements along the tube length (a) and the tube mainstream thickness (b).

It can be seen in Fig. 7(a) that, as in standard acoustic models, the error decreases at higher frequencies where more elements are needed to properly represent smaller wavelengths.The errors

obtained when the number of elements in the mainstream region was increased are shown in Fig. 7(b). Surprisingly, the error decrease mainly at lower frequencies when the number of elements in the mainstream region is increased. This behavior is due to the use of a fixed boundary layer thickness based on the maximum frequency of analysis, so that, at lower frequencies, the higher number of elements in the mainstream is actually improving the representation of the particle velocity field within the actual boundary layer.

4. Conclusion

By studying the viscothermal acoustic propagation on a simple tube, it was shown that the choice of FE discretization can considerably improve the convergence of the results and decrease the computational costs of the FE viscothermal acoustic model (LNSF). It was seen that the discretization of the boundary layer region is very important to obtain an accurate description of the viscothermal effects on the acoustic wave propagation. The analysis of the discretization along the tube length has demonstrated that it is important to properly represent the acoustic wavelength, as well known in standard acoustic FE. In the analysis of the boundary layer discretization, it was observed that the parameterized mesh gives an uniform reduction of the error over the whole frequency range by increasing the number of elements along the boundary layer. This is in contrast with the situation where a fixed discretization (based on the boundary layer thickness at the maximum frequency) was used for the whole frequency range, although this approach can be used as a first estimative of the response.

REFERENCES

[1] M. Bruneau, Ph. Herzog, J. Kergomard, and J. D. Polack. General formulation of the dispersion equation in bounded visco-thermal fluid, and application to some simple geometries. *Wave Motion*, 11(5):441 – 451, 1989.

[2] W. M. Beltman. *Viscothermal wave propagation including acousto-elastic interaction*. PhD thesis, Universiteit Twente, Enschede (the Netherlands), 1998.

[3] C. Zwikker and C. W. Kosten. *Sound absorbing materials*. Elsevier, Amsterdam, 1949.

[4] H. Tijdeman. On the propagation of sound waves in cylindrical tubes. *Journal of Sound Vibration*, 39:1–33, March 1975.

[5] M. Malinen, M. Lyly, P. Raback, A. Kärkkäinen, and L. Kärkkäinen. A finite element method for the modeling of thermo-viscous effects in acoustics. In *Proc. ECCOMAS*, 2004.

[6] M.J.J. Nijhof, Y.H. Wijnant, and A. de Boer. An acoustic finite element including viscothermal effects. In *Fourteenth International Congress on Sound and Vibration, ICSV14*, July 2007.

[7] W. R. Kampinga, Y. H. Wijnant, and A. de Boer. A finite element for viscothermal wave propagation. In *Proceedings of ISMA 2008*, pages 4271–4278, 2008.

[8] AB Comsol. *COMSOL Multiphysics user's guide*, 3.5a edition, 2009.

[9] W. R. Kampinga, Y. H. Wijnant, and A. de Boer. Performance of several viscothermal acoustic finite elements. *Acta acustica united with Acustica*, 96(1):115–124, 2010.

[10] D. T. Blackstock. *Fundamentals of physical acoustics*. John Wiley & Sons, Inc., 2000.